Numerical Study on the Resistance Characteristics and Rotordynamic Coefficients of a Helically Grooved Annular Seal

Yaoyu Hu[1], Yongxiang Lin[2], Dezhong Wang[1,*], Fangming Miu[2], Junlian Yin[1]

[1]School of mechanical engineering, Shanghai Jiao Tong University, No. 800, Dongchuan Rd., Shanghai, China.

[2]Powerchina SPEM Limited Company, No. 80, Hangdu Rd., Shanghai, China.

*email: dzwang@sjtu.edu.cn

Abstract. Helically grooved annular seal can be used as the impeller ring in a pump system to control the leakage from the high pressure impeller outlet to the relatively low pressure suction region. The seal will bring radial forces into the rotor system of the pump, making a significant impact on the rotordynamic characteristics. The radial forces could be expressed by a set of rotordynamic coefficients which are the mass, damping and stiffness coefficients. The rotordynamic coefficients have strong correlation with the resistance characteristics of the seal. Numerical simulations are performed on several helically grooved annular seals to evaluate their resistance characteristics. The simulations are carried out on several seal configurations within a range of pressure differences, rotor speeds and groove depths. The results of the simulations are presented and discussed. The associated rotordynamic coefficients of the seal are determined based on the empirical coefficients obtained from the analysis of the seal resistance. The results indicate that the empirical coefficients are no longer constant and are speed dependent. Furthermore, the rotordynamic coefficients are evaluated using the speed-dependent empirical coefficients.

1. Introduction

The rotordynamic characteristics of a pump are of great importance because the safety is the primary issue for power generation industry. The rotordynamic characteristics of a pump are affected by the fluid confined in the clearance (e.g., seal, impeller ring) between the rotor and the stator. The fluid in the clearance generates radial forces on the rotor. As summarized in [1], the fluid induced forces could be expressed in terms of the rotordynamic coefficients, equation (1)

$$\begin{Bmatrix} f_x \\ f_z \end{Bmatrix} = -\begin{bmatrix} M & m \\ -m & M \end{bmatrix} \begin{Bmatrix} \ddot{x} \\ \ddot{z} \end{Bmatrix} - \begin{bmatrix} C & c \\ -c & C \end{bmatrix} \begin{Bmatrix} \dot{x} \\ \dot{z} \end{Bmatrix} - \begin{bmatrix} K & k \\ -k & K \end{bmatrix} \begin{Bmatrix} x \\ z \end{Bmatrix} \tag{1}$$

where M, C and K are the direct mass, damping and stiffness coefficients, respectively. And, m, c, and k are the cross-coupled counterparts. In equation (1), f_x and f_z are the radial force components, x and z are the displacements of the rotor along the two axes of the coordinate system (assume that the rotor is rotating along y-axis).

One category of the clearances between the rotor and stator inside a pump is the annular seal. The annular seal could take various configurations. In this work the helically grooved annular seal is studied. It is the current design of a main feed water pump for a steam generator system.

In the 1960s, several theoretical and experimental researches were conducted, *e.g.* [2], [3]. Those early work were aiming at exploring the inertial effects of the turbulent flow inside the seals and the resistance or leakage characteristics of the seals.

Lots of important work on both the leakage and rotordynamic characteristics of seals can be attributed to Childs. Under the cooperation with NASA, Childs *et al.* had done a series of work on helically grooved annular seals [4]-[7]. The bulk-flow model developed by Hirs [8] was adopted in the analysis done by Childs *et al*. The rotordynamic coefficients described in equation (1) are obtained by theoretical and experimental analysis.

At the same period of time, Iwatsubo, Yang, *et al.* [9], also based on the theory of Hirs, performed theoretical analysis for the rotordynamic coefficients of helically grooved annular seal. From the studies of Childs and Iwatsbo one can conclude that the resistance of a helically grooved annular seal is affected by various factors. Furthermore, there are possibilities of optimization for specific seals.

The research effort on the helically grooved annular seal has been reduced since 2000s. The reason may be that the helically grooved annular seal may not be the best choice compared to other seal configurations if both the leakage and rotordynamic stability are the primary concern. Lots of researches are for the spiral or herringbone grooved bearing and spiral grooved face seals [10], [11].

Computational fluid dynamics (CFD) techniques have been widely used in the analysis for the seals, particularly when the geometries of the seals are relatively complex compared to seals like the plain annular or labyrinth seals. Rhode, *et al.*[12], Athavale, *et al.*[13], Moore, *et al.*[14] and Untaroiu, *et al.*[15] all employed CFD technique in their work.

In this work, a set of helically grooved annular seals are analyzed by CFD techniques. The seals have groove structures on both the rotor and stator surfaces. Three configurations with different groove depths are simulated. The resistance and the rotor dynamic characteristics are revealed.

2. Computation Model

2.1. Seal geometry and operating condition

The seal under study is an eight-head helically grooved annular seal with both the rotor and the stator grooved. As illustrated in Figure 1, the groove shape (rectangular) and associated parameters are the same between the rotor and the stator, except that the directions of helix are different. For the rotor, the groove follows the right-hand rule along the *y*-axis. Here, the right-hand rule along the *y*-axis means that the helix line goes in the negative *y*-direction while the rotor is rotating along the *y*-axis. The helix angle of the groove is small and has the value of about 1.41 °. The other parameters are listed in Table 1.

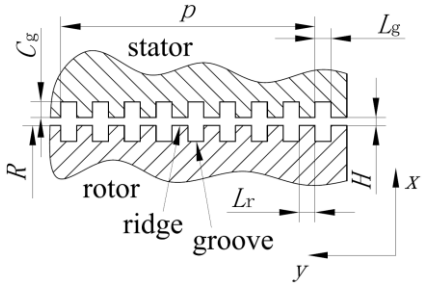

Figure 1. Schematic diagram of the helically grooved annular seal.

As shown in Table 1, there are three groove depths for the seals. The following simulation analysis are performed on these seals with different groove depths.

Table 2 shows the operating conditions of the pump. Water is the working fluid. It should be noted that there are several operating conditions with different running speeds and axial pressure differences. Some of the operating conditions are simply set in this way to perform a parametric study for a better understanding of the characteristics of the seal.

Table 1. Geometry parameters.

Description	Value
Radius, R (m)	0.1555
Length, L (m)	0.05
Nominal clearance, H ($\times 10^{-3}$m)	0.57
Groove width, L_g (m)	0.0015
Ridge width, L_r (m)	0.0015
Groove depth, C_g ($\times 10^{-3}$m)	0.5, 1.0, 1.5
Helix pitch, p (m)	0.024
Helix angle, α (°)	1.41

Table 2. Operating conditions.

Description	Value
Working fluid	
Temperature (℃)	180
Density, ρ (kg/m^3)	891.32
Dynamic viscosity, μ (Pa s)	1.507×10^{-4}
Operating parameters	
Running speed (RPM)	2450, 3675, 4900
Axial pressure difference (MPa)	0.2, 0.3, 0.4, 0.5, 0.8

2.2. CFD Model

As illustrated in Figure 2, 1/8 of the fluid field is separated out since the helically grooves have the eight-head pattern. The separated region is divided into the rotor and stator regions. This strategy lowers the difficulty of meshing the 1/8 fluid field with hexahedron grids considering the different directions of helix. The grids are generated using the ICEM software. Figure 3 shows the grid detail near a groove on the rotor. The thickness of the first layers of grids near the walls are configured to be 1×10^{-6}m. The seal clearance is discretized into 36 elements (with 18 elements on each region). More information is listed in Table 3. The following computations are performed by the CFX software.

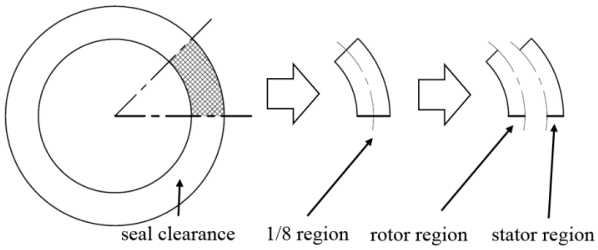

Figure 2. Computational regions.

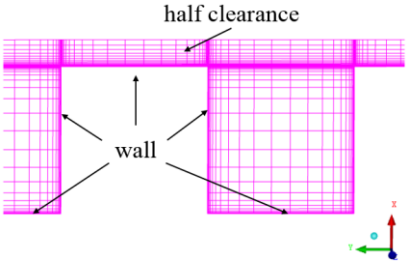

Figure 3. Mesh detail.

The boundary conditions are shown in Figure 4 and Figure 5. Static pressure conditions are set on the inlet and the outlet of the fluid field. The outlet is configured as 'opening' to account for the reverse flow due to the rotation of the rotor. The rotor surface is set to be rotating wall. The surface of the stator is set as stationary wall. Both the rotating and stationary walls are non-slip walls.

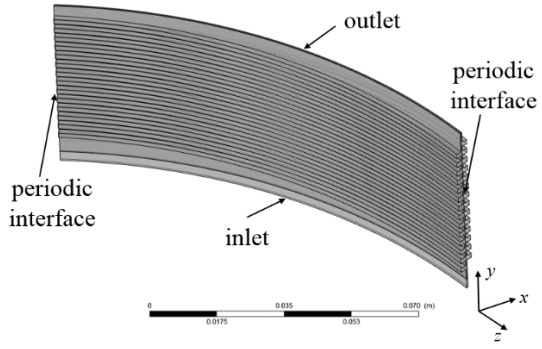

Figure 4. Overall boundary conditions.

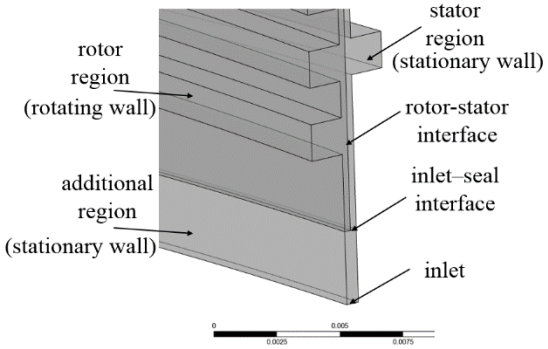

Figure 5. Boundary conditions near the inlet.

Table 3. Grid information.

groove depth (m)	grids of rotor (million)	grids of stator (million)	grids of add. region (million)
0.5	329.40	329.40	23.76
1.0	344.28	344.28	23.76
1.5	360.72	360.72	23.76

In order to overcome the convergence difficulties that arise from possible reverse flow, an additional inlet region (3mm long) is positioned in front of the seal, as shown in Figure 5. The rotor and stator surfaces of the additional region are both set to be stationary non-slip walls. The exchange of the physical variables between fluid regions are realized by the interface technique of CFX. There are three interface pairs in the model: the rotational periodic interface, the interface between the rotor region and the stator region and the interface between the seal and the additional inlet region.

The RNG k-ε turbulent model with wall function is adopted. It is configured that convergence is achieved if the RMS residuals drop below 1×10^{-5}. Moreover, the torque on the seal rotor, the radial force applied on the seal rotor and the averaged velocity on the outlet surface are also monitored. In total, 45 cases are computed in the following section.

3. Simulation Results

3.1. General parameters

The axial flow rates and the torques on the rotor are presented in Figure 6 and Figure 7. Generally, the axial flow rates or the leakages become higher with lower rotating speed. This could be attributed to the so called 'pump effect' of the helically grooves. However, the axial flow rates of different running speeds do not vary substantially. The reason may related to the small helix angle which reduces the pump effect. Among the seals, the 0.5mm-deep groove always leaks the least. It is observed that the axial flow rates of the 1.5mm-deep groove are slightly lower than the 1.0mm-deep groove. These results indicate that the leakage of the seal does not have monotonous relation with the change of the groove depth. From Figure 7, one can find that the torques become larger with higher pressure differences and the deeper the groove is, the higher the operating torque could be expected.

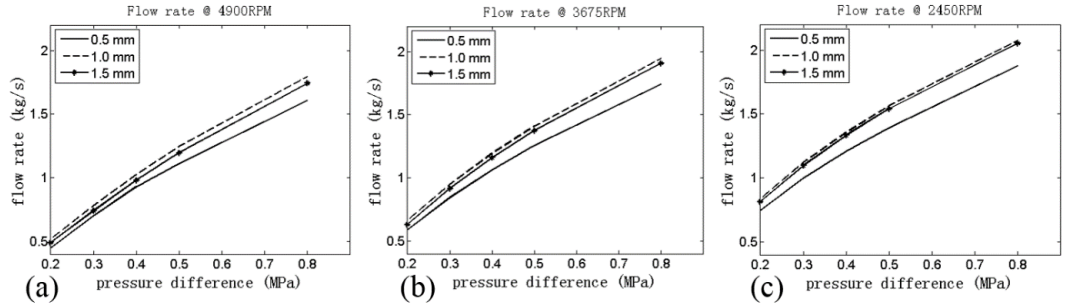

Figure 6. Axial flow rates.

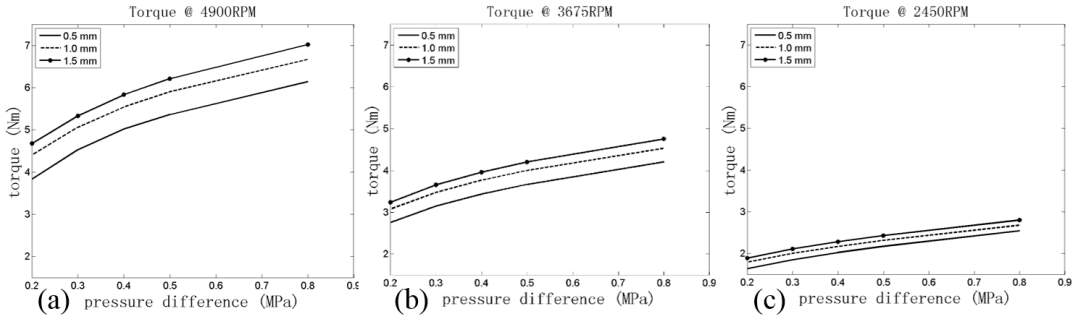

Figure 7. Torques on the rotor.

3.2. Seal resistance

When the fluid passes through the seal, the axial velocity of the fluid and the pressure drop could be correlated by equation (2)[16].

$$\Delta p = \sigma \rho V^2 \tag{2}$$

where Δp is the pressure drop, ρ is the density and σ is the friction loss coefficient. Two cross-section planes are created to help with calculating the pressure drops. These two planes are located just before

the first groove and after the last groove. The pressure drop is evaluated by subtracting the averaged static pressure on these planes. Figure 8 shows the σ coefficients calculated from the numerical results. In Figure 8, the horizontal axis is the axial Reynolds number, which is expressed by equation (3).

$$Re = \frac{\rho VH}{\mu} \tag{3}$$

where H is the nominal clearance of the seal, μ is the dynamic viscosity of the fluid. From Figure 8, it is obvious that the resistance is strong when the running speed is relatively higher. This is consistent with the flow rate results shown in Figure 6. As expected, the seal with the groove depth of 0.5mm has the largest σ values indicating that its resistance is the maximum among all the cases studied.

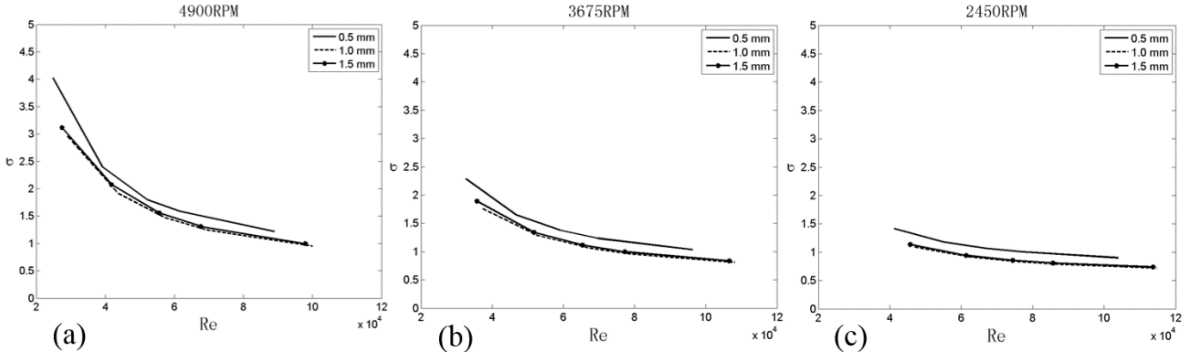

Figure 8. σ coefficients.

4. Rotordynamic coefficients calculation

The rotordynamic coefficients in equation (1) could be determined by the method of Childs [16]. In this method the bulk-flow model of Hirs [8] is used, as equation (4).

$$\frac{\tau}{\frac{1}{2}\rho U^2} = n\left(\frac{\rho UH}{\mu}\right)^m \tag{4}$$

where τ is the shear stress, U is the averaged circumferential velocity, m and n are the empirical coefficients. m and n can be attained by experiments or CFD techniques[17]. In the method proposed by Childs[5], once the empirical coefficients are obtained, they are treated as constants in the following rotordynamic coefficients analysis. This methodology is generally correct as long as the running speed of the rotor is constant. However, the rotordynamic analysis for a pump requires that the rotordynamic coefficients of seals are calculated in a wide range of running speeds. Therefore, the empirical coefficients could not be considered as speed independent. In the present study the empirical coefficients at several running speeds are calculated. Then, the rotordynamic coefficients are estimated by the methodology of Childs using the speed dependent empirical coefficients.

4.1. Empirical coefficients

Following the procedures of Childs[5], the σ coefficient is expressed by equation (5).

$$\sigma = \frac{L}{H} nRe^m \left(1 + \frac{1}{4b^2}\right)^{\frac{1+m}{2}}, b = \frac{V}{R\omega} \tag{5}$$

where Re is the axial Reynolds number, ω is the rotor running speed with the unit of rad/s.

The empirical coefficients could be evaluated by means of least square fit of equation (5). Table 4 lists the values of m and n for different conditions. From Table 4, some trends can be summarized: (1) For seals with groove depths of 1mm and 1.5mm, the values of m become lower. (2) It is likely that seals working at lower running speeds may have positive m values. (3) The m values for seal with 0.5mm groove depth fluctuate with ascending running speeds, while all the m values for the other two seals having monotonous relation with running speeds.

Table 4. Empirical coefficients.

running speed (RPM)	groove depth 0.5mm		groove depth 1mm		groove depth 1.5mm	
	m	*n*	*m*	*n*	*m*	*n*
2450	0.0612	0.0044	0.0054	0.0071	-0.0077	0.0085
3675	0.0804	0.0032	-0.0669	0.0167	-0.0924	0.0235
4900	-0.3220	0.4691	-0.3818	0.8675	-0.3066	0.3460

4.2. Rotordynamic coefficients

The mass, damping and stiffness coefficients are obtained at three running speeds by the method of Childs[5]. The *m* and *n* values of associated running speed are used accordingly. The results are shown in Figure 9 (d. means 'direct', c.c. means 'cross-coupled'). In these figures, the rotordynamic coefficients under the axial pressure difference of 0.4 MPa are shown, because it is near the design point of the pump. Furthermore, the inlet loss coefficient and pre-swirl coefficient defined in the Childs' method are assumed to be 0.1 and 0.5.

As illustrated in Figure 9 (a), the direct mass coefficient is significant. The amount of mass brought by the seal to the rotor system has the same magnitude of the nearby rotor segment. As shown in Figure 9 (b), the seal with 1mm groove depth has slightly higher direct damping than the other two configurations. Little deviations of mass and damping coefficients are present among the seals. The stiffness coefficients show relatively larger differences in Figure 9 (c). The cross-coupled stiffness coefficients are of the same magnitude of the direct stiffness coefficients. This is not favorable because the cross-coupled stiffness destabilizes the pump rotor. Generally, the rotordynamic coefficients (except some of the direct damping coefficients) increase with increasing running speed.

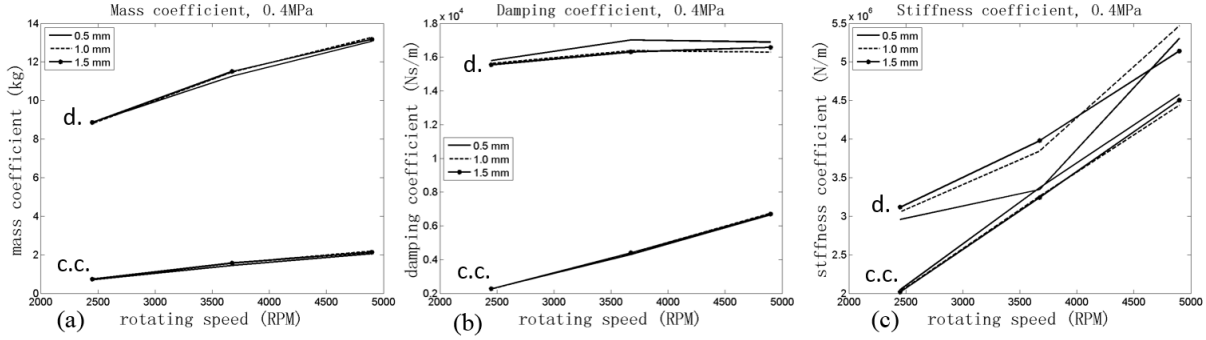

Figure 9. Rotordynamic coefficients.

5. Discussion

In the original work of Childs and Hirs, the empirical coefficients, *m* and *n*, are constants. In most of their studies, the value of *m* is negative. The negative *m* means that the value of σ should decrease with increasing axial velocity. This phenomenon is verified by experiments on plain annular seals [18]. However, positive *m* value dose exist [4]. If the positive constant nature of the *m* value holds for increasing axial flow rates, the σ coefficient may become so large that it leads to extremely unacceptable predictions. Therefore, the state of positive *m* value could only be temporary, respecting the varying axial flow rates due to the change of pressure difference. Furthermore, this study shows that for a helically grooved annular seal, the *m* and *n* values are also not constant when the running speed alters. The values recorded in Table 4 suggest that the sign of the *m* value may vary with the running speed. This situation may be attributed to the pump effect of the seal. Table 4 also indicates that the 0.5mm groove depth has the largest resistance in the speed range lower than 4900 RPM because it has positive *m* or negative *m* with small absolute value.

The results of the present analysis are compared with the rotordynamic coefficients obtained with constant empirical coefficients. The pump under study has its designed operating condition around 4900 RPM, so the values of *m* and *n* at 4900 RPM are utilized. As illustrated in Figure 10 ('c.' and

's.d.' mean 'constant' and 'speed dependent'), the mass coefficients with constant empirical coefficients are higher than the speed dependent ones with maximum deviation of about 10%. The direct damping coefficients with constant empirical coefficients are about 8% lower at the running speed of 2450 RPM, as described by Figure 11. The most dramatic change is in Figure 12, where about 40% over estimation may exist. Small difference is found between the cross-coupled coefficients (Figure 13). The above results suggest that non-negligible deviations of rotordynamic coefficients may arise if the empirical coefficients are treated as speed independent. The cross-coupled mass and cross-coupled damping coefficients are not considered, either because their low numerical values or they are supposed to have little effect on the rotordynamic characteristics of the rotor.

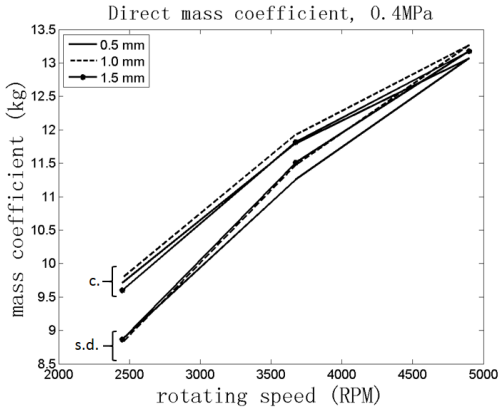

Figure 10. Comparison of mass coefficients.

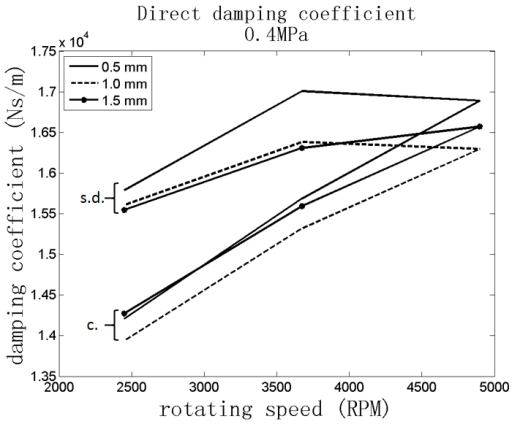

Figure 11. Comparison of damping.

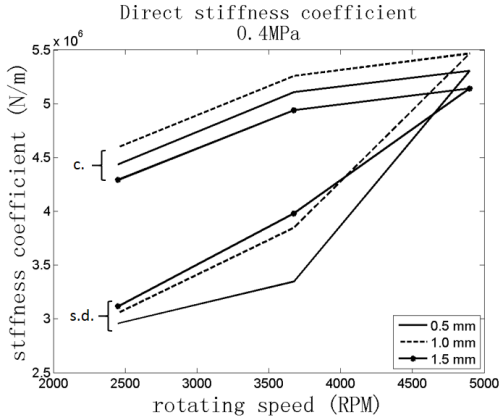

Figure 12. Comparison of direct stiffness.

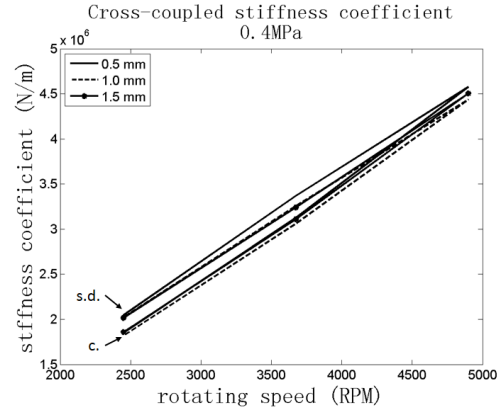

Figure 13. Comparison of cross-coupled stiffness.

6. Conclusion

The following conclusions could be summarized.

- The seal with 0.5mm groove depth has higher resistance than the other seal configurations. However, deeper groove does not always mean larger leakage.
- The torque to drive the rotor increases with increasing running speed. The seal with 1.5mm groove depth demands the largest torque.
- The empirical coefficients of the bulk-flow theory are obtained. It is found that the *m* values of the empirical coefficients are positive under certain seal geometry and operating conditions.
- The rotordynamic coefficients are calculated with speed dependent empirical coefficients. The mass coefficients of the seals are significant. The seals can provide certain damping effect. The cross-coupled stiffness has the same magnitude of the direct stiffness, and they both increase with increasing running speed. Small differences of rotordynamic coefficients are present among seals with various groove depths, except the direct stiffness coefficients.

- The rotordynamic coefficients calculated with speed dependent and constant empirical coefficients are compared. The results show significant deviations. Therefore, it is more reasonable to treat the empirical coefficients as speed dependent.

Acknowledgments
This work is funded by the National Natural Science Foundation of China (No. 51406114 and No. 51576125).

References
[1] Brennen C 2011 *Hydrodynamics of Pumps* (New York: Cambridge University Press)
[2] Zuk J, Strom T, Ludwig L, Johnson R 1967 Convective Inertia and Gas Ingestion Effects on Flow Regimes of the Viscoseal Theory and Experiment *A S L E Trans.* **10** 273
[3] Vohr J and Chow C 1969 Theoretical analysis of spiral-grooved screw seal for turbulent operation *J. Tribol.-T. ASME* **91** 675
[4] Childs D 1983 *The SSME seal test program: Leakage tests for helically-grooved seals* (Turbomachinery Laboratory, Texas A&M University)
[5] Kim C, Childs D 1987 Analysis for rotordynamic coefficients of Helically-Grooved turbulent annular seals *J. Tribol.-T. ASME* **109** 136
[6] Childs D, Nolan S and Kilgore J 1990 Test results for turbulent annular seals, using smooth rotors and helically grooved stators *J. Tribol.-T. ASME* **112** 254
[7] Childs D and Gansle A 1995 Experimental leakage and rotordynamic results for helically grooved annular gas seals ASME 1995 *Int. Gas Turbine and Aeroengine Congress and Exposition. American Society of Mechanical Engineers (Houston, Texas, USA, 5–8 June 1995)* Paper No. 95-GT-179 pp V005T14A009
[8] Hirs G 1973 A bulk-flow theory for turbulence in lubricant films *J. Tribol.-T. ASME* **95** 137
[9] Iwatsubo T, Yang B and Ibaraki R 1987 Theoretical approach to obtaining dynamic characteristics of noncontacting spiral-grooved seals *NASA. Lewis Research Center Rotordynamic Instability Problems in High-Performance Turbomachinery* pp 155-188(SEE N 87-22199 15-37)
[10] Jang G H and Chang D I 2000 Analysis of a hydrodynamic herringbone grooved journal bearing considering cavitation *J. Tribol.-T. ASME* **122** 103
[11] Zhao Y M, Hu J B and Wei C 2014 Dynamic Analysis of Spiral-Groove Rotary Seal Ring for Wet Clutches. *J. Tribol.-T. ASME*, **136** 031710
[12] Rhode D, Hensel S and Guidry M 1992 Labyrinth Seal Rotordynamic Forces Using a Three-Dimensional Navier-Stokes Code. *J. Tribol.-T. ASME* **114** 683
[13] Athavale M, Hendricks R, Steinetz B 1995 Numerical Simulation of Flow in a Whirling Annular Seal and Comparison with Experiments, *the 31st Joint Propulsion Conf. and Exhibit (San Diego, California, United States, 10-12 July)*
[14] Moore J 2003 Three-Dimensional CFD Rotordynamic Analysis of Gas Labyrinth Seals. *J. Vib. Acoust*. **125** 427
[15] Untaroiu A, Hayrapetian V, Untaroiu C, Wood H, Schiavello B, McGuire J 2013 On the Dynamic Properties of Pump Liquid Seals. *J. Fluids Eng.* **135** 051104
[16] Childs D and Kim C 1985 Analysis and testing for rotordynamic coefficients of turbulent annular seals with different, directionally-homogeneous surface-roughness treatment for rotor and stator elements *J. Tribol.-T. ASME* **107** 296
[17] Keith G, Bhattacharjee P, Nielsen K, Ha T, Childs, D, Platt J 2009 Friction factor jump in honeycomb seals explained by flow-acoustic interactions *ASME Turbo Expo 2009: Power for Land, Sea, and Air. ASME (Orlando, Florida, United States, 8-12 June 2009)* pp GT2009-60337
[18] Yamada Y 1962 Resistance of a flow through an annulus with an inner rotating cylinder *Bulletin of JSME* **5** 302